Investigation of Cake Fouling and Pore Blocking Phenomena Using Fluid Dynamic Gauging and Critical Flux Models

William J. T. Lewis[a], Tuve Mattsson[b,c], Y. M. John Chew[a,d]* Michael R. Bird[a,d]

[a] *Department of Chemical Engineering, University of Bath, Claverton Down, Bath, BA2 7AY, UK.*
[b] *Department of Chemistry & Chemical Engineering, Chalmers University of Technology, SE-412 96 Gothenburg, Sweden.*
[c] *Wallenberg Wood Science Center, The Royal Institute of Technology, Chalmers University of Technology, SE-100 44 Stockholm, Sweden.*
[d] *Centre for Advanced Separations Engineering, University of Bath, Claverton Down, Bath, BA2 7AY, UK.*

* *y.m.chew@bath.ac.uk*

Abstract

Cake growth during a low pressure cross-flow microfiltration (MF) of a Kraft lignin suspension was studied using fluid dynamic gauging (FDG). The FDG results were used to quantify the significance of pore-level fouling phenomena which occur at an early stage of the filtration. We present here a novel toolset for quick and achievable diagnosis of membrane fouling mechanisms, which can accelerate innovations in membrane technology and process optimisation. A flux decline of approximately 75% was attributed to pore level fouling i.e. deposition on the surface of the membrane which caused direct blocking of the membrane pores. This is the first time FDG measurements of cake thickness have been used to isolate pore-level fouling phenomena. Furthermore, this innovative approach showed good agreement with a mathematical approach, based on a critical flux model, which was applied to raw flux data. In addition to cake thickness measurements, destructive strength testing of the fouling layer showed an increase in cohesive strength over time. The results showed that filter cakes formed by Kraft lignin become harder to remove by shear stress as they become thicker during the course of the filtration. The methodology described here can be applied to rapidly predict and assess routes to performance improvements in cross-flow MF.

Keywords: cake fouling, Kraft lignin, critical flux, cohesive strength, thickness, microfiltration

1. Introduction

In membrane filtrations, fouling is defined as the unwanted deposition of material on or within the membrane. It results in a loss of performance, indicated either by a rise in transmembrane pressure (TMP), or a drop in flux. Cross-flow filtrations are the method of choice for a majority of industrial filtrations, as they are intended to reduce or control fouling through

fluid shear at the surface of the membrane. However, this does not usually eliminate the problem. In some cases it may be impracticable to induce enough shear to completely remove or prevent fouling, while in others various particle-membrane interactions which lead to fouling cannot be overcome.

The exact nature of fouling is difficult to ascertain, as this would require some form of observation and measurement in addition to its effects alone. One approach that has been explored is to develop models which use fluid-particle dynamics to describe the transport of rejected particles in a filtration system towards, or away from the membrane. The constant pressure filtration laws developed by Hermia [1] are often used to describe foulant accumulation in dead-end filtrations. Models to describe back-transport away from the membrane in cross-flow filtrations include inertial lift [2,3] and shear-induced diffusivity [3,4]. Such models rely on predictable and uniform particle characteristics, and often do not consider particle-membrane and inter-particle interactions, reducing their applicability to more complex foulants. Lewis [15] compared such models with experimental studies of particle re-entrainment from a filter cake, highlighting how they become inappropriate for removal of existing cakes.

This work presents a practical approach to study cake growth on microfiltration (MF) membranes. An automated fluid dynamic gauging (FDG) technique [5] was used to track the thickness and strength of cake layers. This is applied to the cross-flow MF of lignin, a substance which has earlier been found to be relatively self-adhesive [6]. Using this data it is possible to infer how fouling phenomena at the surface of the membrane and in a growing cake fouling layer on top influence flux decline individually. In addition to this, the capacity to interrogate flux data for similar evidence is also explored, using principles originally derived from the constant pressure blocking laws of Hermia [1]. For the first time, FDG studies have been used as a means to estimate the impact of pore fouling phenomena Analysis presented in this work is based on that provided by Field *et al.* [7] on the critical flux concept.

Field *et al.* [7] postulated that there exists a critical flux for cross-flow filtrations, below which no fouling will be observable by its effect on filtration performance e.g. flux decline or increased TMP. While this concept could be debatable – some authors have observed membrane fouling before any noticeable decline in performance [8], and others have reported membrane fouling after prolonged operation below a critical flux [9] – it remains a helpful guideline for designing continuous filtration operations. In addition to the experimental evidence from which they derived the critical flux concept, Field *et al.* [7] produced an analytical model, based upon Hermia's [1] pore blocking laws (which built upon those of Hermans and Bredee [10]), namely:

$$-\frac{dJ}{dt}J^{n-2} = k(J - J^*) \tag{1}$$

where J is flux, t is time, n and k are constants specific to the type of blocking law as summarised in Table 1, and J^* is the limiting flux for the specific blocking law. The different fouling laws concerned are cake filtration, intermediate, and complete blocking (wherein n increases from 0 to 2 respectively). The mechanics of each type of blocking law are discussed thoroughly in numerous other publications [1,7,11].

Table 1. Constants used in equation (1) for three different fouling models, where φ_c is the cake specific resistance, k_c' is a cake filtration constant, J_0 is initial flux, R_m is the membrane resistance, σ is the blocked membrane surface area per unit volume of permeate, and ε_m is the membrane surface porosity. [7]

Fouling law	k	n
Cake Filtration	$\frac{\varphi_c k_c'}{J_0 R_m}$	0
Intermediate blocking	σ	1
Complete Blocking	$\frac{J_0 \sigma}{\varepsilon_m}$	2

This model supposes that pore blocking, then intermediate blocking, and finally cake filtration take place sequentially, not simultaneously. For each type of blocking law, the limiting flux, J^*, would be that below which, for a constant transmembrane pressure, no fouling of this kind would occur.

If one defines a function of flux as:

$$f(J) = -\frac{dJ}{dt}J^{n-2} \tag{2}$$

it follows that equation (1) will be valid when a linear relationship between $f(J)$ and J is observed [12]. Hence one could infer the type of fouling mechanism (e.g. $n = 0$, 1, or 2), limiting flux J^* for that particular mechanism, and estimate parameters such as those included in k, which are shown inTable 1. A detailed explanation of the way in which this equation is applied is given in the appendix A1.

In this work, the fouling of MF membranes with Kraft lignin is investigated, with particular interest paid to the growth and structure of cake fouling layers formed by this material. Equation (1) is used to discern the point at which initial fouling of the membrane surface (e.g.

complete then intermediate blocking), gives way to cake fouling. In this way it is possible to estimate the significance of the two former mechanisms within the overall resistance of a fouling layer. This can be represented in the resistance-in-series model:

$$J = \frac{TMP}{\mu\left(R_m + R_c + R_p\right)} \tag{3}$$

where μ is the viscosity of the permeate, R_m is the membrane resistance, R_c is the resistance of the cake fouling layer, and R_p is the resistance at pore-level. Here we combine the resistance generated by intermediate and complete blocking into a single resistance value, R_p.

2. Materials and Methods

Fluid dynamic gauging (FDG) experiments were performed to estimate the thickness change of cake layers during the course of cross-flow filtration, as well as providing information about their local cohesive strength. FDG is a technique which relies on simple fluid dynamic principles of flow constriction to estimate the thickness of fouling deposits [13]. In this case pressure-mode FDG is used, wherein liquid is drawn into a nozzle, see Figure 1 (a), suspended above the fouled surface (e.g. above the cake-fouled membrane). The pressure drop, Δp_g, into this nozzle due to the constriction between its tip and the top surface, of the foulant gives an indication of its clearance, h, which, knowing the position of the nozzle relative to the membrane, h_0, can be used to infer the thickness of the fouling layer. A detailed explanation of FDG and its use in this context is given in [5] and [14].

2.1 Apparatus

An FDG probe was installed on a purpose-built MF test section in a feed and bleed flow loop, each of which are described below. The entire system was controlled and monitored by connection to a data-logging PC, using a LabView visual interface (VI). A fuller description of this apparatus is given in [5].

2.1.1 Test section

A schematic of the test section used in this work is shown in Figure 1 (b). It contains a small rectangular flow channel with a membrane as the bottom surface, allowing for cross-flow filtrations. The feed side of the channel is 16 mm high and 15 mm wide. The membrane is secured in a removable stainless steel cassette (inset), in which it is sandwiched between a rubber seal and rigid stainless steel mesh spacer. The available membrane surface in the cell is 150 mm long, giving a total filtration area of 0.00225 m^2.

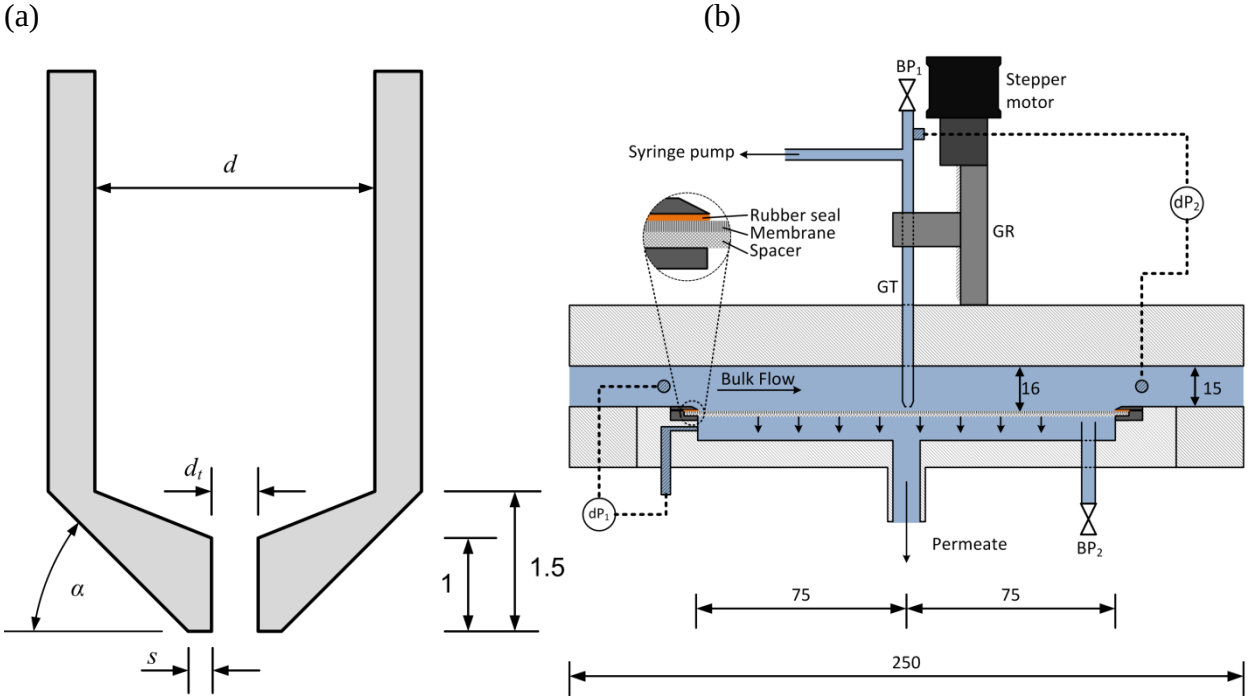

Figure 1. (a) Diagram of FDG nozzle, where d is the inner diameter of the gauge tube, d_t is the nozzle orifice diameter, α is the external taper angle of the nozzle, and s is the radial width of the gauge nozzle rim. (b) Schematic of the test section, where dP_1 and dP_2 are pressure transducers, BP_1 and BP_2 are bleed points with pinch valves, GR is a linear guide rail and V7 is a needle valve used to control TMP. GT is the gauge tube, which includes the gauge nozzle on the end described in (a). All stated dimensions are in mm. Reprinted from [15].

2.1.2 FDG Probe

The gauging nozzle is installed directly at the centre of the test section, with dimensions, referring to Figure 1 (b), of d = 3 mm, d_t = 0.5 mm, α = 45°, and s = 0.25 mm. Gauge height is controlled with a guide rail and stepper motor, and monitored using a linear variable differential transformer (SM-series LVDT, *RS Components* ± 0.5 µm). A detailed description of this component assembly is given in [5].

2.1.3 Flow loop

The test section was installed in the flow loop shown in Figure 2. Process fluid from a well-mixed feed tank was circulated through the system using a regenerative pump (HPR 6/11, *Totton*) through a variable area flowmeter (Rotameter Series 1100, *KDG Instruments*) and 500 mm long, 15 mm square entry section prior to the test section. Permeate from the membrane was discharged at atmospheric pressure and weighed using a digital balance (FX-3000i, *A&D* ±0.005 g), retentate was recirculated back to the feed tank. Valves V2 and V5 were adjusted to control the flowrate through the test cell (characterised by a Reynolds number, Re_{duct}, for the entry section) and V7 was used to control TMP. A differential transducer, dP_1 (PX26-005DV,

±1 mbar, *Omega Engineering*) was used to monitor the TMP. A syringe pump (Touchscreen 100 series, *Cole-Parmer*) was used to control flow through the FDG tube, m_g, and a pressure transducer, dP_2 (PX26-001DV, ±0.25 mbar, *Omega Engineering*) was used to measure Δp_g for use in thickness estimations.

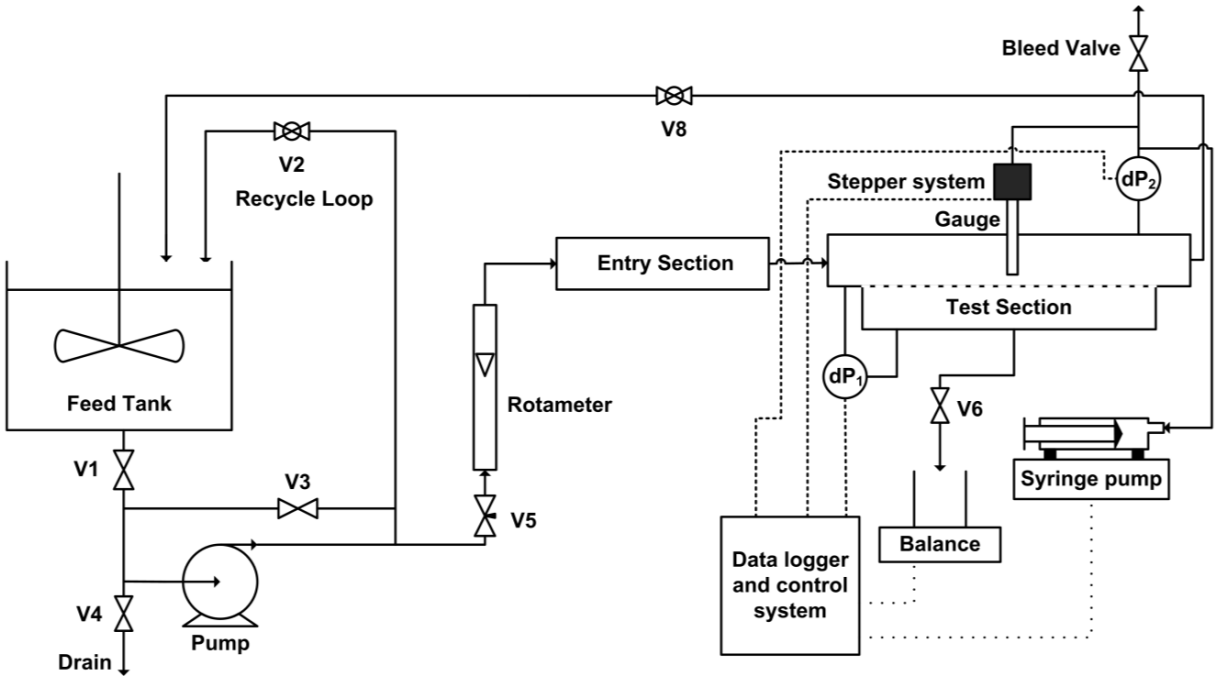

Figure 2. Flow loop used in this work where V1-V7 are valves, and dP_1 and dP_2 are pressure transducers (as indicated in Figure 1a). Reprinted from [15].

2.2 Materials

2.2.1 Feed suspension

The feedstock used in these filtrations was a washed Lignoboost™ softwood Kraft lignin. This chemically modified lignin which is soluble in alkaline solution is recovered by precipitation under acidic conditions, and subsequently washed [16]. It is produced during the delignification of wood for the purpose of Kraft pulp production (a process common to paper milling). The Kraft lignin used in this study has been double-washed for purity. A total volume of 15 litres of 0.02 vol% suspension was prepared from a 2 vol% stock slurry. The stock slurry was prepared from powdered lignin, and stirred for at least 24 hours prior to use so that the particles were sufficiently dispersed. Reverse osmosis (RO) water, adjusted to pH 3.7 using sulphuric acid, was the liquid medium in all suspensions. This lowered pH was adopted to ensure that lignin particles were insoluble. Solids density for dried lignin particles was measured at 1350 $kg \cdot m^{-3}$ using a gas pycnometer (AccuPyc II 1340, *Micromeritics*). A particle size

distribution was also taken for each filtration experiment (MasterSizer X, *Malvern*) to ensure relatively consistent suspension characteristics.

Notable variations in size of the solid lignin agglomerates, herein referred to as particles, were recorded between experiments. However, this was not found to cause an impact in the filtration behaviour of the suspension. Table 2 shows the average and span of each measure of characteristic diameter, while FigureFigure 4 shows particle size distributions for suspensions representative of the minimum, average and maximum $d_{(50)}$ values. This are correspondingly labelled low, medium and high. Some variation between experiments was unavoidable; however the peak particle size remained consistent at around 3 μm. The greatest variation was observed in the size range of larger particles which appear as a result of incomplete dispersion, and/or agglomeration over time. This is evidenced numerically by the range of $d_{(90)}$ values.

Table 2. Average, maximum, and minimum particle size data for all experiments. $d_{(x)}$ values indicate the particle diameter for which x vol% are smaller.

	$d_{(10)}$ (μm)	$d_{(50)}$ (μm)	$d_{(90)}$ (μm)	$d_{(3,2)}$ (μm)	$d_{(4,3)}$ (μm)
Minimum	1.70	5.40	24.80	3.70	11.00
Average	1.75	6.18	30.26	4.08	12.83
Maximum	1.90	8.60	60.30	5.00	19.90

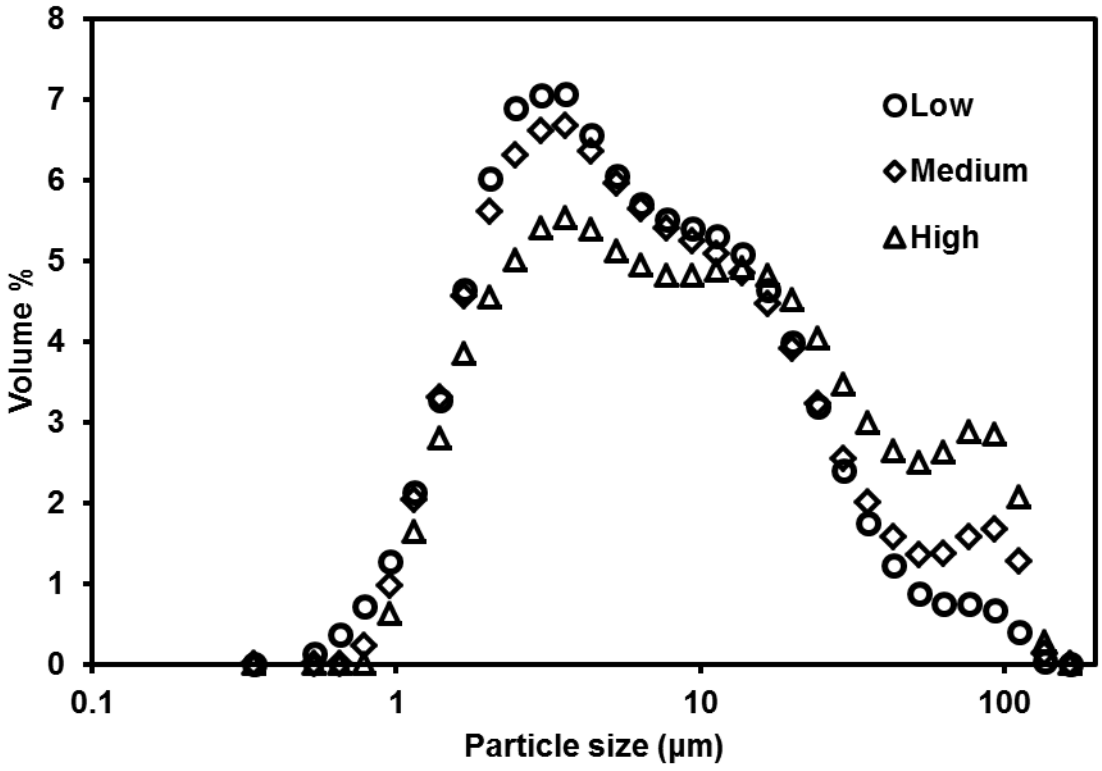

Figure 3. Particle size distributions of selected lignin suspensions representative of low, medium and high average particle size. Distributions with maximum and minimum $d_{(50)}$ values are shown as the high and low data. The suspension which most closely matches the mean $d_{(50)}$ value is shown here as the medium average particle size.

2.2.2 Membranes

Regenerated cellulose membranes, which are hydrophilic, symmetric, and contained no wetting agents, of nominal pore size 0.2 μm (RC58, *Whatman*) were selected for complete rejection of lignin. A new membrane sample was used for each experiment, which was prepared by soaking in RO water for at least 30 minutes before installation in the test section. Although the nominal pore size of the membranes was lower than the smallest agglomerate size in the suspension, SEM images of the membrane surface shown in Figure 4 clearly indicate recesses larger than some of the particles in suspension. Membrane resistance, R_m, was characterised by dead-end filtration using the method and apparatus described by [14].

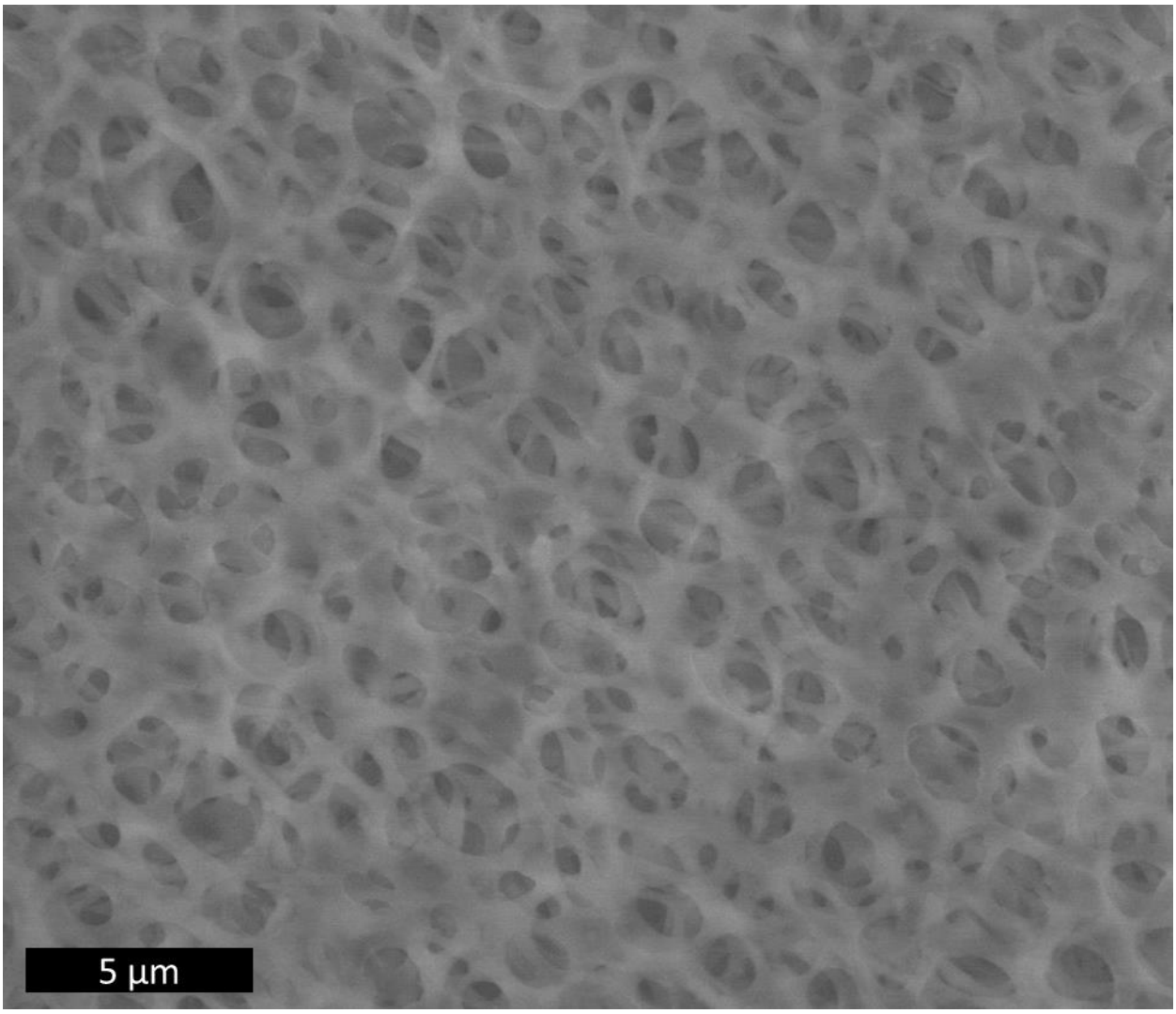

Figure 4. SEM image of microfiltration membrane used in this work. Image taken using a Quanta 200 FEG, *FEI*. The sample was not coated prior to imaging

2.3 Methods

All filtration experiments were performed under the same conditions, namely a TMP of 100 mbar, and cross-flow velocity characterised by a Reynolds number for the entry section of 1550. This gave a cross-flow velocity of 0.1 m s^{-1}. In order to achieve a reliable measure for cake growth, the method developed by Lewis *et al.* [5] was employed. The FDG technique is used only once during the course of a filtration to, in addition to making cake thickness estimates, perform destructive strength tests on the cake at a chosen time point in the filtration. In doing this it is possible to gain an insight into the varying structure of the cake layer over time as well as its thickness. The procedures involved for each filtration experiment are described below.

2.3.1 FDG Calibration

A 14 L volume of pH adjusted RO water was used to prime the system, and flowrate and TMP were set using manually controlled valves and the pump. Prior to fouling of the membrane, a Δp_g vs. h_0 profile was produced. The gauging flow, m_g, was started by activating the syringe pump with the gauge position about 2 mm from the surface of the membrane. The gauge was moved to a position ~ 0.5 mm from the membrane, and then stepped incrementally towards the surface, taking a pressured reading Δp_g at each step, only when steady values were achieved, as evidenced by 5 successive readings within 0.6 mbar of each other. This entire process was automated, and completed before the syringe was filled. Afterwards the gauge was retreated to a position ~10 mm from the surface to avoid interference with cake fouling. Fluid was then slowly ejected from the syringe back into the feed side of the test section. All measurements were taken at a gauging flowrate of $m_g = 0.1$ g·s^{-1}.

The Δp_g vs. h_0 profile was then used to ascertain the position of the membrane relative to the FDG nozzle, as this can change by small amounts for each filtration when a new membrane is mounted [5]. In addition, poor calibration profiles could be used to indicate incorrectly or loosely mounted membranes or other irregularities in the apparatus before running an experiment.

2.3.2 Filtrations and Thickness measurements

At the commencement of a filtration run, 1 L of diluted feedstock was added to feed tank under constant mixing. Filtrations were run in feed and bleed mode, with permeate being retained outside of the test cell. Although this should typically result in an increased retentate concentration, a small decrease by ~1.2% was observed over the course of a 4000 s filtration. This is discussed further in the results section. Measurements were made only after a specific filtration time had elapsed, in order to prevent influence on cake growth by FDG. Filtration times of 750, 1000 and 2000 s were used to give an indication of cake growth over time. Between 7 and 8 runs were performed for each time. Singular experiments were performed for times of 3000 and 4000 s. For each thickness measurement, the syringe pump was activated, withdrawing fluid from the test cell at a rate of $m_g = 0.1$ g·s^{-1}. The gauge was moved to within 2 mm distance from the membrane, at which point the gauging flow was commenced, and the gauge moved stepwise towards the surface until steady pressure readings were achieved at a value indicating that $h/d_t \sim 0.2$.

Following this reading, destructive strength testing was performed. The FDG nozzle was moved in 20 µm steps towards the membrane, and in smaller steps as it became closer, until a

maximum Δp_g (limited by the pressure transducer) value was read, indicating a nozzle clearance of $h/d_t = 0.06$ ($h = 30$ μm). At each step a reading was taken at a steady-state when 5 successive Δp_g values within 0.6 mbar variation were recorded. At each of these steady-states, some of the fouling layer directly beneath the FDG nozzle has been removed due to fluid shear forces imposed on the cake surface by gauging flows. The remaining material is that which is resilient to shear forces caused by FDG at the current clearance, the thickness of which is estimated by FDG. Thus it is possible to estimate the cohesive strength at various positions from the surface of the cake layer towards the membrane.

After this destructive strength testing the test section was drained slowly, and any water remaining removed through the membrane. The fouled membrane was then retrieved, and the foulant was rinsed into a petri dish, dried and weighed for comparison with thickness data. The dry weight of deposit was adjusted to account for extra material captured when draining the test section.

3. Results

3.1 Flux Decline and Cake Thickness

Although 7 or 8 experiments were performed for each filtration time of lignin, some datasets were discarded through a two-tier selection process. A consistent flux decline profile was seen in almost all experiments. Behaviour in aberrance of this was suggestive of an improperly secured membrane, or contamination of the feed during filtration. Examples of the flux decline curves are shown in Figure 6, and data which showed a notable deviation from the profile exhibited in the majority of filtrations was discarded. The second criteria was based on cake volume fraction. When calculated using thickness measurements, low estimates suggest that large particulates have been swept off the surface of the membrane before making the first thickness reading. To avoid unreasonable estimates in cake thickness, data from which significant outliers from a linear trend between cake thickness and deposited mass per unit area were also discarded. Due to the low TMP during filtrations, no significant cake compression is expected in these experiments.

Starting fluxes averaged at 1900 $L \cdot m^{-2} \cdot h^{-1}$, with a maximum allowed deviation of 160 $L \cdot m^{-2} \cdot h^{-1}$. The small increase in flux evident at the start of the experiment was due to a small head increase in the feed tank upstream of the pump when the lignin feedstock was added. The flux shown in Figure 5 shows the standard asymptotic profile expected of a cross-flow filtration. A steady-state flux value was not reached in these experiments. Nor so was a steady value for cake thickness, which appears to increase almost linearly with time from 1000 seconds onwards.

It should be noted that the error margin for 3000 s of approximately 9 μm is quite high in Figure 5 because a measurement was recorded at a higher h/d_t value than at 4000 s.

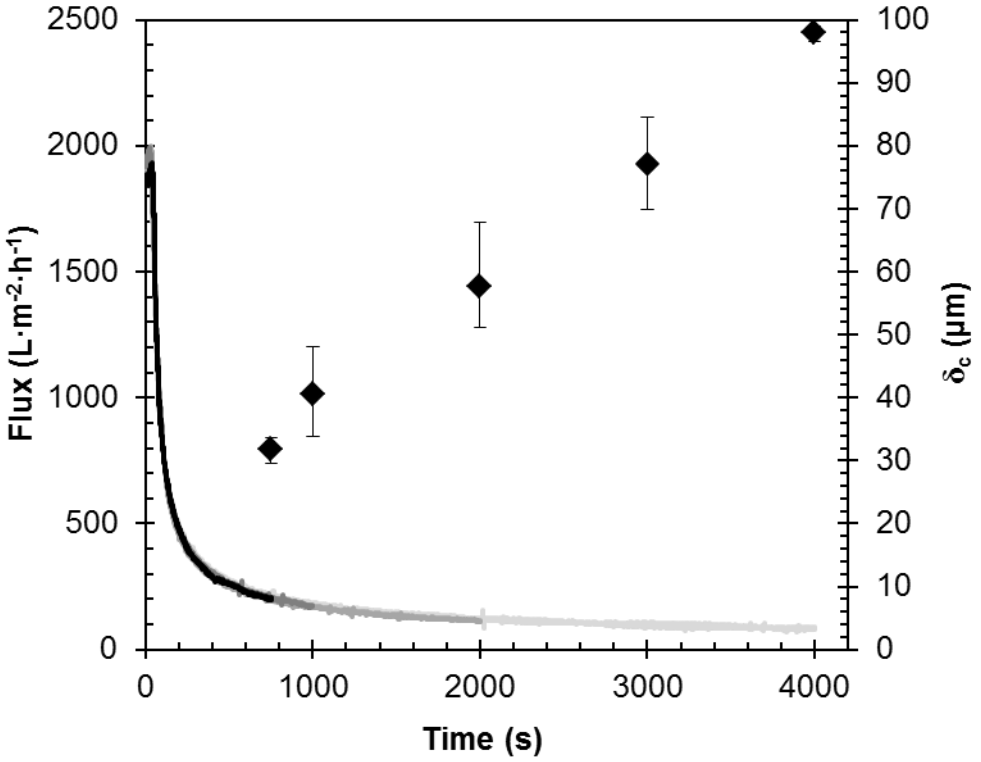

Figure 5. Cake thickness (symbols) and flux (lines) vs. time. Error bars for 750, 1000, and 2000 s indicate span of data across repeat experiments. Those for 3000 and 4000 s indicate measurement error. The black, dark, medium and light grey lines indicate flux curves for separate experiments ending at times 750, 1000, 2000 and 4000 seconds respectively

3.2 Analysis of cake resistance

A fouling resistance, R_f, defined as:

$$R_f = \left(R_c + R_p\right) = \frac{TMP}{\mu J} - R_m \tag{4}$$

was determined from flux by rearrangement of equation (3). This is plotted against the cake thickness, δ_c in Figure 6. A linear regression fit was produced, and extrapolated back to $\delta_c = 0$. The intercept here can be interpreted as pore-level fouling resistance, R_p, i.e. that which can be attributed to complete and/or intermediate blocking. With $R_p = 5\times10^{10}$ m^{-1}, and $R_c = 0$, a flux of approximately 500 L·m^{-2}·h^{-1}is predicted by equation (3). This is reached within 200 s filtration time, hence it is very plausible that pore-level fouling phenomena have a strong influence on this filtration.

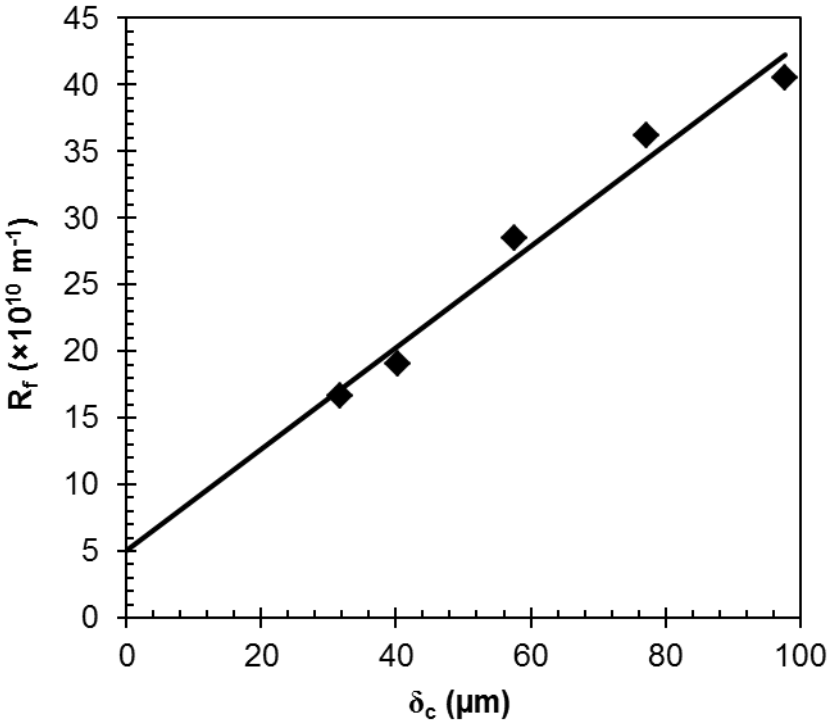

Figure 6. Fouling resistance, R_f, against cake thickness. The line indicates a linear regression fit. Values shown here are from average thickness and flux data where multiple valid experiments were considered (e.g. for 750, 1000 and 2000 s).

3.3 Destructive Thickness tests

Destructive thickness tests indicated possible changes in the cohesive strength of the cake over time. Cake thickness is plotted against the maximum shear stress imposed by the gauge, $\tau_{w,max}$, in Figure 7. $\tau_{w,max}$ has been shown to occur near the inner edge of the nozzle rim [5]. The graphs show data for all valid experiments considered. The thinner cakes formed in shorter, 750 s filtrations exhibited some degree of swelling or stretching under the shear force imposed by the gauge, as indicated by Figure 7 (a), where the cake grows by approximately 10 μm between 30 and 70 N·m^{-2}. This effect is seen for one of the 1000 s experiments, shown by triangles in (b), and not at all for the thicker cakes at filtrations of 2000 s and above. This could indicate stretching or other deformation of the cake layer without removal.

A general negative trend is seen in all these results, showing that layers of cake closer to the membrane surface are harder to remove than those at the top of the cake i.e. the cohesive strength increases as the cake gets thinner. Comparison between figures 7 (a), (b), and (c) clearly shows how thicker cakes, or at least those developed over longer filtrations, exhibit less repeatable results. Some unexpected behaviour is also indicated in (d) for the cake formed over a 3000 s filtration. Here a cake layer of 37 μm thickness remains at a shear stress of 270 N m^{-2}, however the cake is subsequently eroded, decreasing $\tau_{w,max}$. Further increases in shear stress

lead to a final cake thickness estimation of 21 μm at the maximum stress measured. This is likely due to the sudden removal of a more sizeable layer of cake, which not only reduced cake thickness but also h, resulting in a lower shear stress. $\tau_{w,max}$ was subsequently increased by moving the gauge closer to the surface.

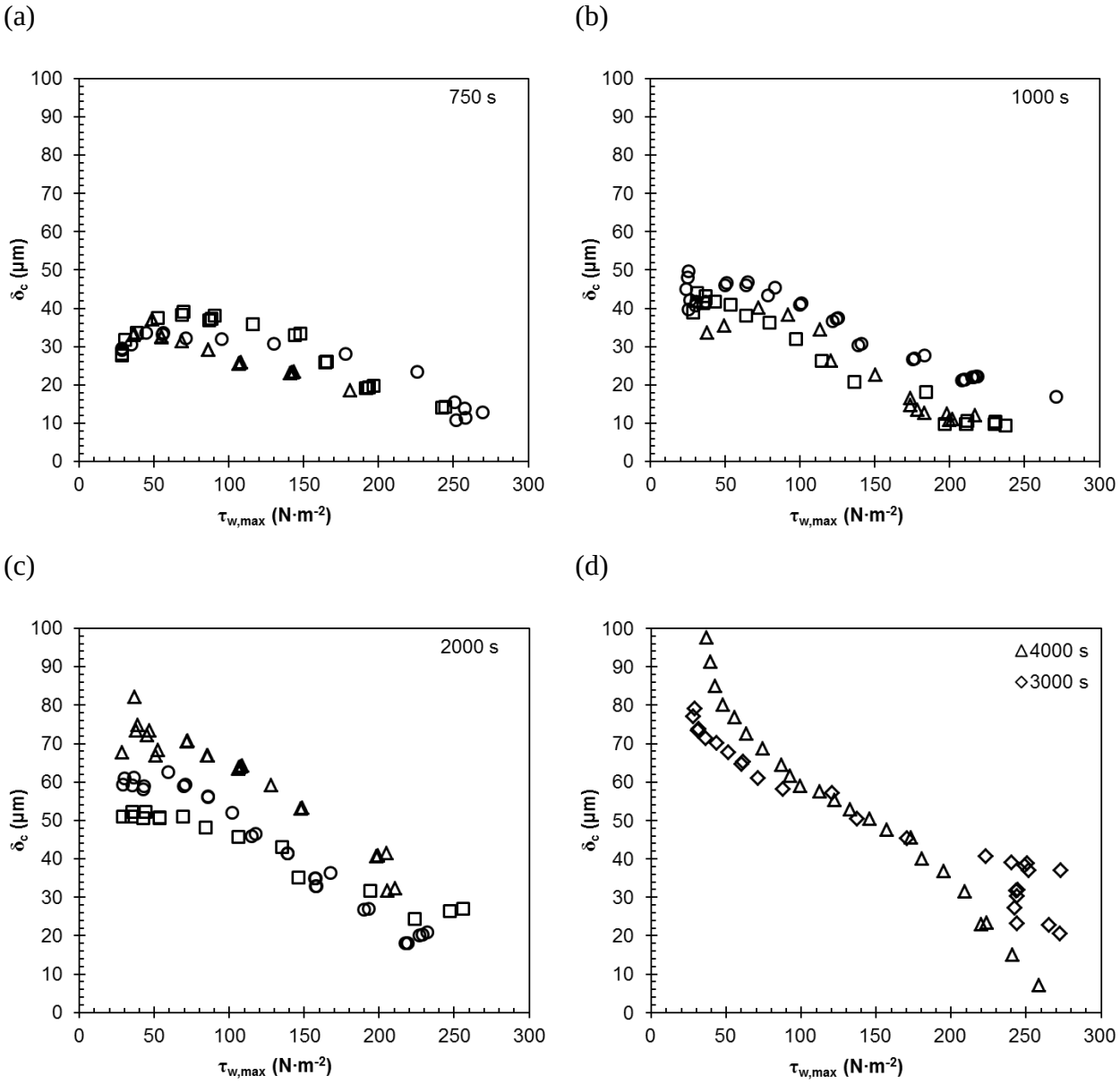

Figure 7. Thickness vs. maximum wall shear stress, $\tau_{w,max}$, for lignin cakes fouled for (a) 750, (b) 1000, (c) 2000, and (d) 3000 and 4000 seconds. Results for all experiments considered valid are shown here.

In no cases does this data indicate the cake is entirely removed, as at the maximum imposed shear stress in all these studies a residual fouling layer of a thickness between about 10 and 20 μm is implied by the data. Although it was possible to image this fouled surface from above using a microscope, the material deposited when draining the system obscured the morphology of the eroded region. In similar fouling studies using the same apparatus, Mattsson *et al.* [17] were able to produce such an image under slightly different conditions. The authors

found a similar formation to that presented by Lewis et al. [5], of a tapered crater-like morphology. There is a possibility that the apparent 10-20 μm layer of cake suggested by Figure 7 is a result of the geometry of this crater-like formation. The mechanism by which this might occur is discussed more thoroughly in [5]. Mattsson *et al.* [17] observed that little or no material remained on the membrane surface after FDG experiments, besides a few specks and some evidence of staining. However, it is uncertain whether these were deposited in the process of recovering the membrane.

So far it has not been possible to clearly ascertain whether a thin layer of particles still measureable within the resolution of FDG, remains on the membrane under the high shear stresses of these destructive tests. Detection of such a layer is non-trivial, and would best be achieved through in-situ optical studies, made more problematic by the non-translucent nature of the feed.

A yield stress, characterised as that above which significant erosion of the cake (due to FDG) is observed. For fouling layers developed over 750, 1000, and 2000 s filtrations this is between 60 and 80 $N \cdot m^{-2}$. However, the shear stress required to remove cake down to a given thickness increases with filtration time. Figure 7 (d) suggests that this yield-stress behaviour is not seen for the longer filtrations. This implies a limiting thickness, above which a weaker cake is deposited, with respect to differing filtration time.

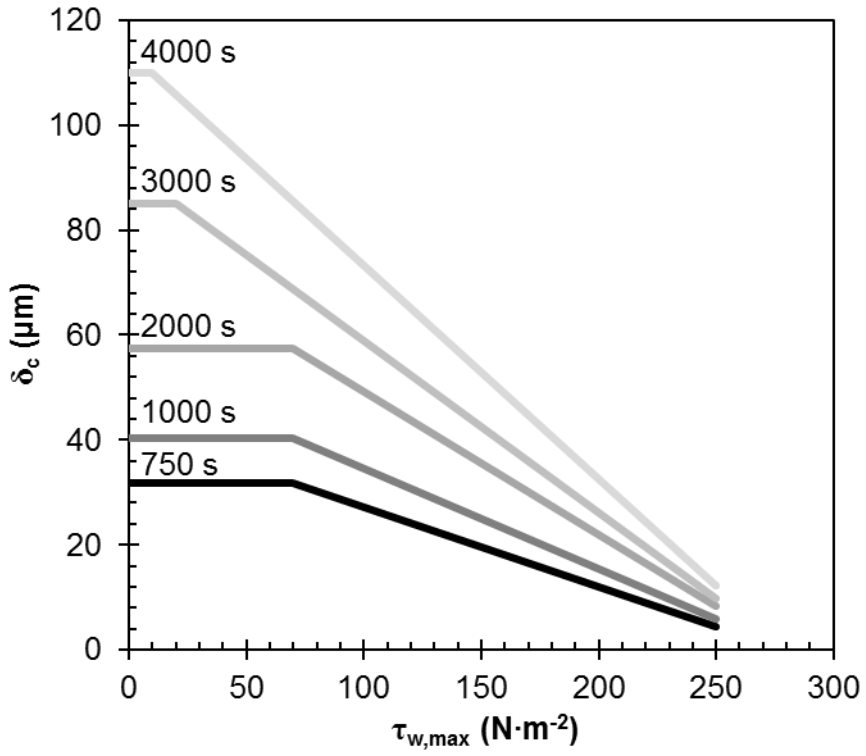

Figure 8. Proposed mechanism for cake erosion under shear stress, with respect to differing filtration times. These lines are predicted as a rough description of the mechanisms which give rise to data shown in Figure 7

A model form for the data above is proposed in Figure 8. From this model, as well as the resistance and thickness data, a mechanism for cake growth is drawn. As more cake layers are deposited during filtration, those lower in the cake rearrange due to being subjected to higher compressible pressure. This makes them more resilient to fluid shear. The result is that after longer filtrations, more stress is required to remove cake down to a particular thickness. The yield point of the cake, required to start removing particles from the surface, is common to all cakes below a limiting thickness. Cake material above this thickness is then much more easily removed. In this model the thickness tends towards zero at a common shear stress value, which can be interpreted as the adhesive strength of the foulant to the surface.

3.4 Application of the Critical Flux Model

The model described by equation (2) was applied to the flux data from this filtration to identify a flux transition point, J_T. As flux drops below this value, the value of n at which equation (2) best fits flux vs. time data switches from 1 (intermediate blocking) to 0 (cake filtration). J_T was determined automatically for each individual set of filtration data by means of a Matlab® script. Details of this algorithm are provided in appendix A2.

It should be noted that positive flux is plotted on the x-axis in Figure 9, so filtration time would move in the direction from right to left. From the algorithm described above, the value of J_T in this particular set was derived to be 365 $L \cdot m^{-2} \cdot h^{-1}$, as indicated in (a). Small variations for this arose across all the data, producing an average of 387 $L \cdot m^{-2} \cdot h^{-1}$. Again assuming that at this point in the filtration $R_c = 0$, equation (3) gives an estimate of pore fouling resistance at $R_p = 9.31 \times 10^{10}$ m^{-1}, which is higher than indicated by FDG measurements (of $R_p = 5 \times 10^{10}$ m^{-1}). However, inspection of Figure 9 (a) suggests an elongated transition between the non-linear and linear zone. This begins at a higher flux, ca. 460 $L \cdot m^{-2} \cdot h^{-1}$. Furthermore, although a reasonable linear trend could not be established for $n = 1$ or $n = 2$, a transition from $n = 1$ to $n = 0$ fouling behaviour is suggested. Figure 9 (b) shows the same flux data using equation (1) with $n = 1$. Here, inspection of the curve suggests a transition at $J = 475$ $L \cdot m^{-2} \cdot h^{-1}$. This predicts pore level resistance more similar to that from using FDG measurements, which was estimated at 5×10^{10} m^{-1}, corresponding to a flux of 500 $L \cdot m^{-2} \cdot h^{-1}$.

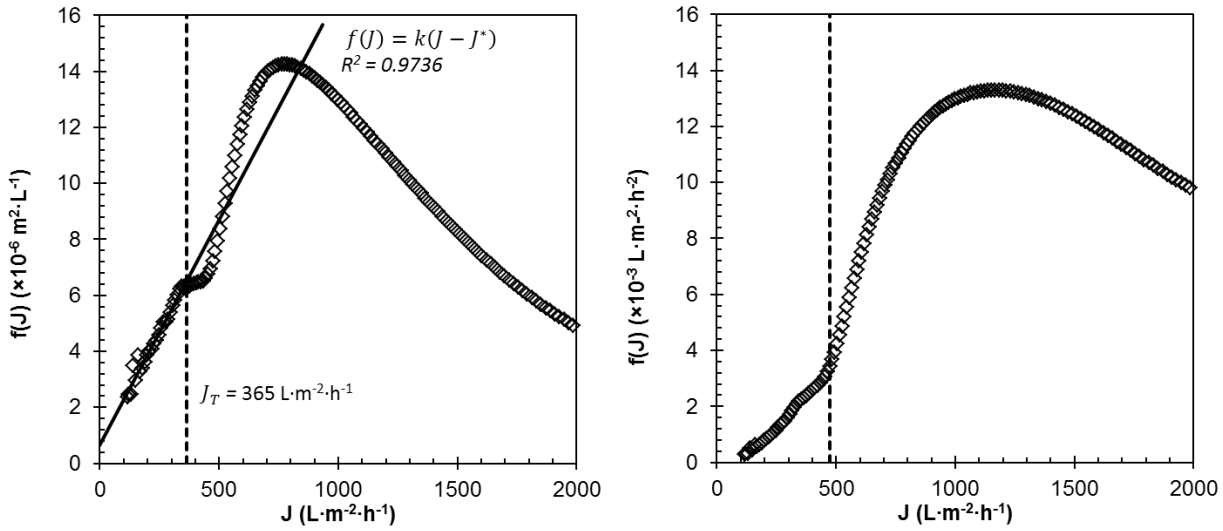

Figure 9. Example data from a 2000 s filtration for $f(J)$ where (a) $n = 0$, and (b) $n = 1$. The solid black line indicates the linear trend identified for data where $J < J_T$ (R^2 is indicated at the top of the line), while the vertical dashed line indicates J_T. $0.9\max(f(J))$ is indicated by the horizontal dashed line. In (a), J_T was estimated procedurally (as described in appendix A), in (b) an estimate is made by inspection.

Hence, it is possible to produce an estimation of the impact of pore fouling phenomena on cross-flow filtration by analysis of flux decline. This aligned reasonably well with that produced through the use of thickness measurements by FDG. That pore openings can become severely constricted is no surprise considering comparisons between the small particle sizes of 1-2 µm present in the suspension, and the surface level pore structure of the membrane shown in Figure 4.

3.4.1 Limiting flux

The value J^* in equation (1) represents the flux at which no fouling will occur under the current filtration conditions. It should be expected that, when $J = J^*$, an equilibrium will be reached at which the rate of cake growth due to convection of particles towards the surface due to flux is matched by their removal due to cross-flow velocity. Given by the y-axis intercept of the linear fit in Figure 9 (a), J^* will be a negative quantity. One implication of this is that extra particle deposition occurs on top of that due to flux, and in excess of any back transport due to cross-flow. This is confirmed by gravimetric analysis, deposited cake mass per unit area of membrane, M_c/A_m, is shown in Figure 10, alongside a curve predicting the same quantity, given by:

$$\frac{M_c}{A_m} = \int_0^t J\, c_b . dt \tag{5}$$

where c_b is the bulk concentration of lignin in the suspension (0.27 kg·m^{-3}). This assumes no back-transport of particles from the membrane. As some of the suspension was drained from the test section through the membrane, some extra deposition was expected. The quantity of lignin within this volume of fluid has been subtracted from the cake mass reported here.

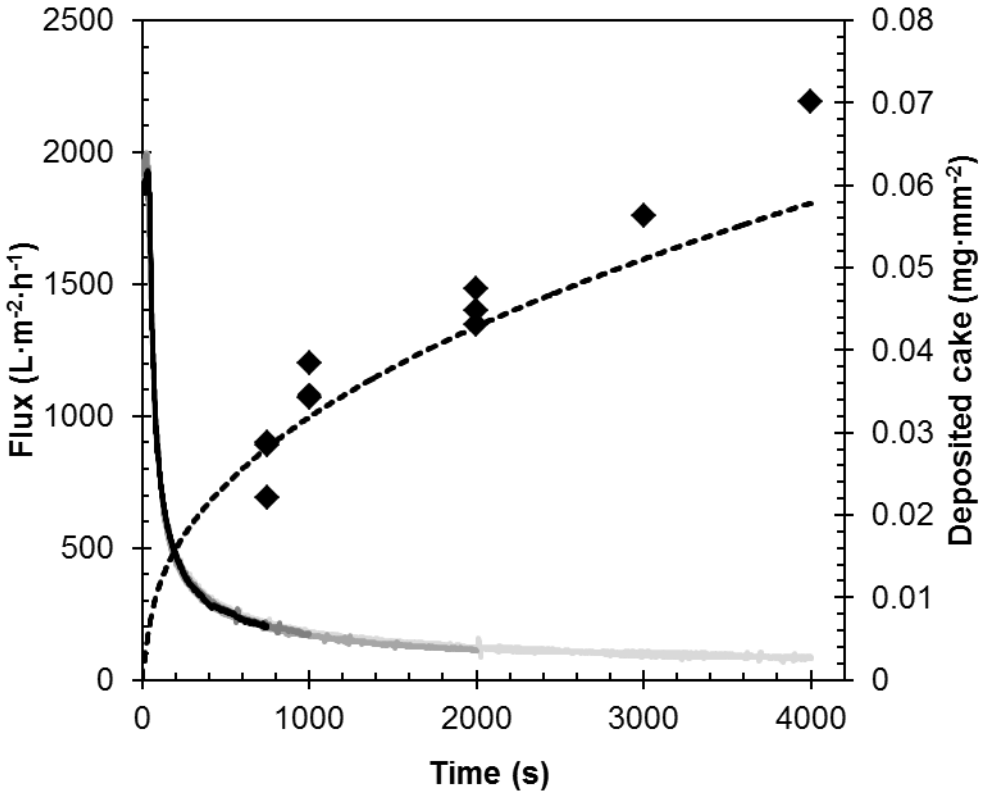

Figure 10. Dry cake mass deposited per unit area of membrane (symbols) and flux (lines) against time. Black, dark, medium and light grey lines represent fluxes for 750, 1000, 2000 and 4000 s respectively. The dashed line indicates the quantity of cake predicted by equation (7) for the 4000 s experiment.

It is evident in Figure 10 that equation (7) under-predicts the deposition of cake mass. Additional capture of particles by the cake may be due to some affinity between lignin particles, and also partially due to settling. We therefore conclude in this work that, not only is it possible to predict the impact of pore-level fouling phenomena using the critical flux formulae, but one can also establish whether additional deposition mechanisms are present.

4. Conclusions

Fluid dynamic gauging was used to estimate cake growth during a lignin filtration at low transmembrane pressure and cross-flow velocity. Thin cakes within 100 μm were formed after 4000 s filtration, which grew almost linearly after an initially fast build-up. Destructive strength testing at different stopping points through the filtration indicated that the cohesive strength of the cake increases over time, as further layers are deposited. A yield strength of 60-80 N·m^{-2} was

observed for cakes up to around 60 μm thick. Above this thickness the top surface of the cake was much more easily deformable.

Using cake growth data a pore-level fouling was inferred to cause a flow resistance of approximately 5×10^{10} m^{-1}, which accounted for an almost 75% decrease in flux at the start of the filtration. Flux data was analysed using Field *et al.'s* [7] modification of constant pressure filtration laws. This produced a similar estimate for the resistance of this layer, and also correctly identified excess cake deposition.

This work demonstrates how a relatively simple FDG study, supported by detailed analysis of flux decline, can provide important information about the nature of fouling in a cross-flow filtration. In this particular case it highlights how most of the loss in filtration performance is likely due to a very thin distribution of particles on the membrane surface. The additional information provided by destructive thickness testing indicated that lignin cakes become less resilient to fluid shear at higher thicknesses, particularly as they approach 100 μm. For this particular filtration, it can therefore be concluded that by restricting fouling phenomena to cake filtration (e.g. by using a membrane with smaller, more regular pores) might improve overall throughput, even if reducing the initial flux.

Appendix

A1 Application of critical flux theory

Figure A1 presents an example of the application of theory discussed in section 1 using artificially generated model flux data. Here data has been generated using equation (1), for which an initial flux, J_0, of 1900 $L \cdot m^{-2} \cdot h^{-1}$ was predefined. The filtration is modelled as having an initial fouling regime where $n = 2$ and then transitions instantaneously to $n = 1$ at 200 s as indicated by the dashed grey line. Another instantaneous transition to $n = 0$ is made at 600 s, as indicated by the dashed black line. The same data is shown by plotting $f(J)$ from equation (2) against flux in (b), (c), and (d), wherein $n =$ 2, 1, and 0 respectively. Here the same dashed lines represent the transitions between fouling mechanisms, this time at the corresponding flux where this transition occurs. For each graph, a linear trend exists only where the fouling law has been applied. For example, in (b) the trend is seen before the grey dashed line indicating J at 200 s, then in (c) the linear trend occurs between J at 200 s and 600 s respectively. Finally, in (d) the linear trend occurs only at fluxes where $t >$ 600 s. For analysis of experimentally generated flux data, plots such as these can be used to determine the approximate flux at which these transitions occur by identifying these linear regions.

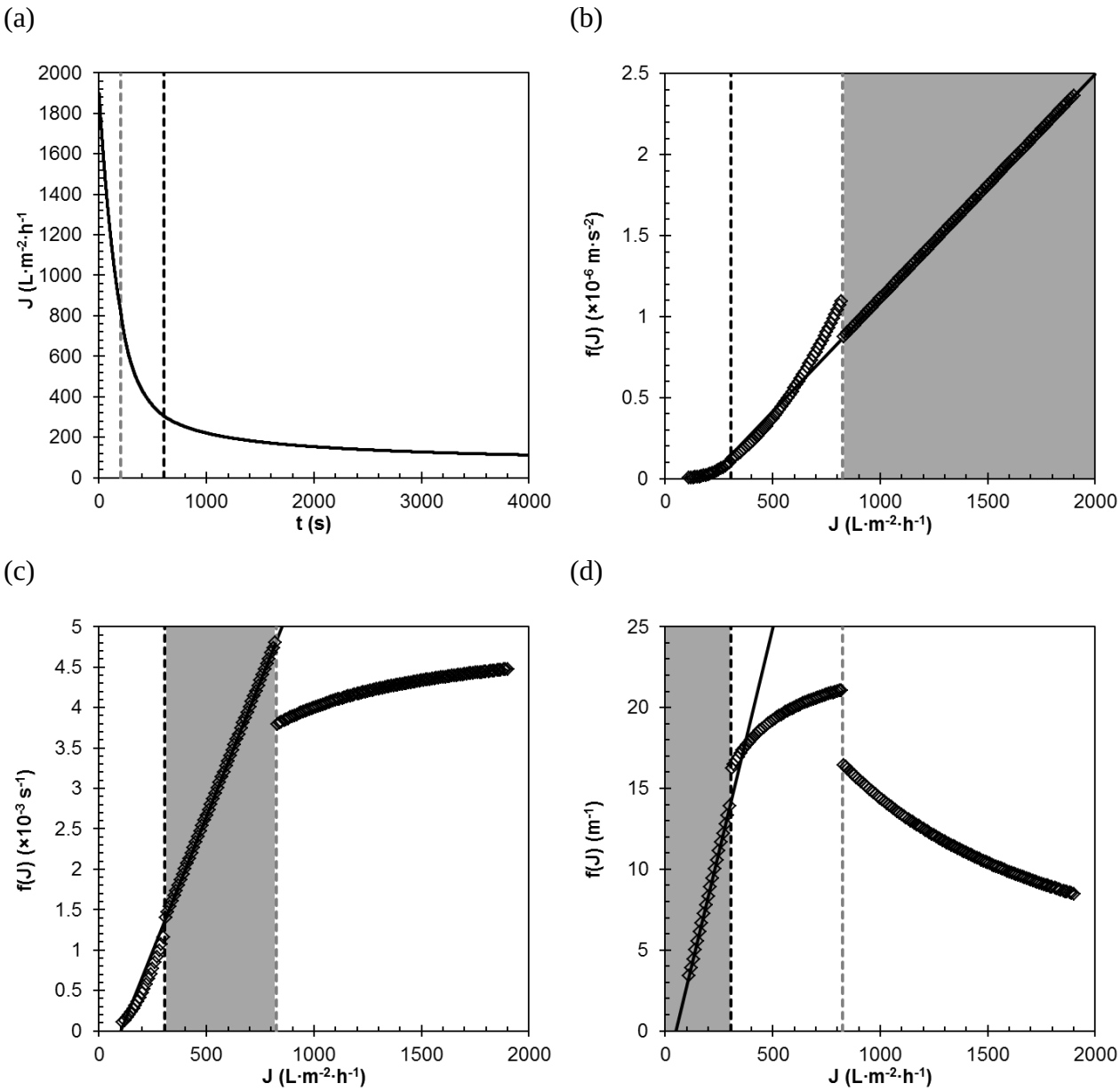

Figure A1. (a) Artificially generated model flux data for a cross-flow filtration following sequential blocking laws as described by equation (1). (b), (c) and (d) Show $f(J)$, as described by equation (2) where n = 2, 1, and 0 respectively. Dashed lines represent time or flux at t = 200 s (grey) and t = 600 s (black).

A2 Data processing script

Using a value of n = 0 in equation (2), $f(J)$ vs. J data was analysed to identify a region of linear trend. An example of this data is shown in Figure 9 (a). Comparison with Figure A1 (d), which exhibits an equivalent plot for model data, shows a good agreement with the general curve shapes in the different fouling regimes. As expected, the sudden transitions between the different fouling regimes do not appear in this experimental data.

Flux vs. time data was processed as follows to determine an appropriate value for J_T:

1. The first 50 s of data were removed due to unsteady readings occurring as the filtration was commenced. So was flux data after the end time for the filtration.
2. Noise was reduced using a spline fit with a smoothing parameter of 10^{-5}.
3. A dataset of 10 000 data points was produced using the resulting curve function
4. The dataset was split into 200 intervals of equal ΔJ
5. dJ/d_t for each interval was determined by linear regression
6. $f(J)$ was determined for each value of J with $n = 0$. Data for $n = 1$ and $n = 2$ showed no clear linear regions so an effective algorithm for their discernment could not be established.
7. The most appropriate value of J_T was determined by iterating through the J values in the dataset in the range $J_{T,min} \leq J_T \leq J_{T,max}$, where $J_{T,min}$ was the value of the fifth data point from the minimum J value, and $J_{T,max}$was the lower of the two J values where $f(J) = 0.9 \max(f(J))$, as indicated by the horizontal line on figure 10 (a).

   Linear regression was performed in the range $J_{final} \leq J \leq J_T$ for each interated J_T value, producing an array of R^2 vs. J_T. The appropriate value of J_T was selected as that corresponding to the highest R^2 value.The resulting linear fit at the selected J_T value was used to determine J^* and k for this filtration.

Nomenclature

J	Flux [L·m^{-2}·h^{-1}]
R	Resistance [m^{-1}]
M	Mass [kg]
A	Area [m^2]
c	Concentration [kg·m^{-3}]
k	Constant used in flux decline model (units vary)
k_c'	Cake filtration constant [kg·m^{-3}]
J_0	Initial flux [L·m^{-2}·h^{-1}]
n	Fouling parameter [-]
J^*	Critical/limiting flux for a particular fouling mechanism [L·m^{-2}·h^{-1}]
t	Time [s]
d	Nozzle tube diameter [m]
d_t	Nozzle throat diameter [m]
s	Nozzle rim width [m]

h	Nozzle clearance from surface [m]
h_0	Nozzle clearance from membrane [m]
m_g	Gauging flowrate [kg·s^{-1}]

Greek lettering

φ_c	Specific cake resistance [m·kg^{-1}]
σ	Blocked membrane surface area per unit volume of permeate [m^{-1}]
ε_m	Membrane surface porosity [-]
δ_c	Cake thickness [m]
Δp_g	Differential gauging pressure [Pa]
$\tau_{w,max}$	Maximum surface shear stress below FDG nozzle [N·m^{-2}]

Subsripts

T	Transition between n = 1 and n = 0
m	Membrane
c	Cake
p	Pore-level
f	Fouling
b	Bulk fluid

References

[1] J. Hermia, Constant Pressure Filtration Laws – Application to Power Law Non-Newtonian Fluids, Trans. Inst. Chem. Eng. 60 (1982) 183–187.

[2] D.A. Drew, J.A. Schonberg, G. Belfort, Lateral inertial migration of a small sphere in fast laminar flow through a membrane duct, Chem. Eng. Sci. 46 (1991) 3219–3224. doi:10.1016/0009-2509(91)85023-Q.

[3] H. Li, A.G. Fane, H.G.L. Coster, S. Vigneswaran, An assessment of depolarisation models of crossflow microfiltration by direct observation through the membrane, J. Memb. Sci. 172 (2000) 135–147. doi:10.1016/s0376-7388(00)00334-3.

[4] C.A. Romero, R.H. Davis, Experimental verification of the shear-induced hydrodynamic diffusion model of crossflow microfiltration, J. Memb. Sci. 62 (1991) 249–273. doi:10.1016/0376-7388(91)80042-5.

[5] W.J.T. Lewis, A. Agg, A. Clarke, T. Mattsson, Y.M.J. Chew, M.R. Bird, Development of an automated, advanced fluid dynamic gauge for cake fouling studies in cross-flow filtrations, Sensors Actuators, A Phys. 238 (2016) 282–296. doi:10.1016/j.sna.2015.12.019.

[6] T. Mattsson, W.J.T. Lewis, Y.M.J. Chew, M.R. Bird, In situ investigation of soft cake fouling layers using fluid dynamic gauging, Food Bioprod. Process. 93 (2015) 205–210. doi:10.1016/j.fbp.2014.09.003.

[7] R.W. Field, D. Wu, J.A. Howell, B.B. Gupta, Critical flux concept for microfiltration fouling, J. Memb. Sci. 100 (1995) 259–272. doi:Doi: 10.1016/0376-7388(94)00265-z.

[8] F. Wicaksana, A.G. Fane, P. Pongpairoj, R. Field, Microfiltration of algae (Chlorella sorokiniana): Critical flux, fouling and transmission, J. Memb. Sci. 387-388 (2012) 83–92. doi:10.1016/j.memsci.2011.10.013.

[9] Y. Ye, V. Chen, A.G. Fane, Modeling long-term subcritical filtration of model EPS solutions, Desalination. 191 (2006) 318–327. doi:10.1016/j.desal.2005.04.128.

[10] P.H. Hermans, H.L. Bredee, Principles of Mathematical Treatment of Constant-Pressure Filtration, J. Soc. Chem. Ind. (1936) T1–T4.

[11] G. Belfort, R.H. Davis, A.L. Zydney, The behavior of suspensions and macromolecular solutions in crossflow microfiltration, J. Memb. Sci. 96 (1994) 1–58. doi:10.1016/0376-7388(94)00119-7.

[12] R.W. Field, J.J. Wu, Modelling of permeability loss in membrane filtration: Re-examination of fundamental fouling equations and their link to critical flux, Desalination. 283 (2011) 68–74. doi:10.1016/j.desal.2011.04.035.

[13] T.R. Tuladhar, W.R. Paterson, N. Macleod, D.I. Wilson, Development of a novel non-contact proximity gauge for thickness measurement of soft deposits and its application in fouling studies, Can. J. Chem. Eng. 78 (2000) 935–947. http://dx.doi.org/10.1002/cjce.5450780511.

[14] W.J.T. Lewis, Y.M.J. Chew, M.R. Bird, The application of fluid dynamic gauging in characterising cake deposition during the cross-flow microfiltration of a yeast suspension, J. Memb. Sci. 405-406 (2012) 113–122. doi:10.1016/j.memsci.2012.02.065.

[15] W.J.T. Lewis, Advanced Studies of Membrane Fouling: Investigation of Cake Fouling Using Fluid Dynamic Gauging, University of Bath, 2014.

[16] F. Öhman, H. Theliander, P. Tomani, P. Axegard, Method for separating lignin from black liquor, 8486224, 2013. http://www.freepatentsonline.com/8486224.html.

[17] T. Mattsson, W.J.T. Lewis, Y.M.J. Chew, M.R. Bird, Investigation of the Formation and Cohesive Strength of Fouling Layers During Cross-Flow Microfiltration using Fluid Dynamic Gauing, 12th World Filtration Congress (2016), Taipei